

Spin decoherence of a heavy hole coupled to nuclear spins in a quantum dot

Jan Fischer,¹ W. A. Coish,^{1,2} D. V. Bulaev,^{1,3} and Daniel Loss¹

¹*Department of Physics, University of Basel, Klingelbergstrasse 82, 4056 Basel, Switzerland*

²*Institute for Quantum Computing and Department of Physics and Astronomy, University of Waterloo, 200 University Avenue W., Waterloo, Ontario, Canada N2L 3G1*

³*Institute of Solid State Physics, Russian Academy of Sciences, 142432 Chernogolovka, Moscow District, Russia*

(Received 30 September 2008; published 31 October 2008)

We theoretically study the interaction of a heavy hole with nuclear spins in a quasi-two-dimensional III–V semiconductor quantum dot and the resulting dephasing of heavy-hole spin states. It has frequently been stated in the literature that heavy holes have a negligible interaction with nuclear spins. We show that this is not the case. In contrast, the interaction can be rather strong and will be the dominant source of decoherence in some cases. We also show that for unstrained quantum dots the form of the interaction is Ising, resulting in unique and interesting decoherence properties, which might provide a crucial advantage to using dot-confined hole spins for quantum information processing, as compared to electron spins.

DOI: [10.1103/PhysRevB.78.155329](https://doi.org/10.1103/PhysRevB.78.155329)

PACS number(s): 72.25.Rb, 03.65.Yz, 31.30.Gs, 73.21.La

I. INTRODUCTION

The spin of a quantum-dot-confined electron is considered a major candidate for the realization of solid-state-based quantum bits,¹ the basic building blocks for quantum information processing devices and, eventually, for a quantum computer.² One of the main obstacles to building these devices is the decay of spin coherence. The ultimate limit to the coherence time for electron spins in most quantum dots at low temperatures is set by the hyperfine interaction with nuclei in the host material.^{3–6} If no special effort is made to control this environment, the associated coherence times are quite short, typically of order nanoseconds.^{4–7}

Very recently, several experiments have shown initialization and readout of single hole spins in self-assembled quantum dots^{8–11} and control over the number of holes in single gated quantum dots:¹² prerequisites for single-hole-spin dephasing-time measurements. Ensemble hole-spin dephasing times have recently been measured in *p*-doped quantum wells.¹³ Hole-spin coherence times in III–V semiconductor quantum dots are anticipated to be much longer than electron-spin coherence times due to a weak hyperfine coupling relative to conduction-band electrons.^{14–21} In the present work, we show that, in contrast, the coupling of a heavy hole (HH) to the nuclear spins in a quantum dot can be rather strong, potentially leading to coherence times that are comparable to those for electrons. However, in the quasi-two-dimensional (Q2D) limit, this interaction takes on a simple Ising form

$$H = \sum_k A_k^h s_z \tilde{I}_k^z, \quad (1)$$

where A_k^h is the coupling of the HH to the k th nucleus, s_z is the hole pseudospin- $\frac{1}{2}$ operator, and \tilde{I}_k^z is the z component of the k th nuclear-spin operator \mathbf{I}_k . The form of this effective Hamiltonian has profound consequences for the spin dynamics. Coherence times can be dramatically extended by preparing the slowly varying nuclear field in a well-defined state (“narrowing” the field distribution).^{6,22–27} For an electron spin interacting with nuclei via the contact hyperfine interac-

tion, narrowing is effective only up to the time scale where slow internal nuclear-spin dynamics or transverse-coupling (flip-flop) terms become relevant. Here we will show that heavy holes confined to two dimensions have negligible flip-flops, potentially leading to significantly longer spin coherence times. The strong coupling of the HH to the nuclear spins is not due to confinement but is also present in bulk crystals, while the Ising-type interaction is a feature of Q2D systems.

This paper is organized as follows: In Sec. II we write down the nuclear-spin interactions and derive an effective spin Hamiltonian for a quantum-dot-confined HH. In Sec. III we calculate the dynamics of the transverse HH spin for different external magnetic-field directions. In Sec. IV we give estimates of the coupling strengths for the special case of a GaAs quantum dot. Conclusions and comparison to recent experiments can be found in Sec. V. Technical details are deferred to Appendixes A–D.

II. NUCLEAR-SPIN INTERACTIONS

A. Hamiltonians

For a relativistic electron in the electromagnetic field of a nucleus with nonzero spin at position \mathbf{R}_k , there are three terms that couple the electron spin and orbital angular momentum to the spin of the nucleus: the Fermi contact hyperfine interaction (h_1^k), a dipole-dipole-like interaction (the anisotropic hyperfine interaction h_2^k), and the coupling of electron orbital angular momentum to the nuclear spin (h_3^k). Setting $\hbar=1$, these interactions are described by the following Hamiltonians:²⁸

$$h_1^k = \frac{\mu_0}{4\pi} \frac{8\pi}{3} \gamma_S \gamma_{j_k} \delta(\mathbf{r}_k) \mathbf{S} \cdot \mathbf{I}_k, \quad (2)$$

$$h_2^k = \frac{\mu_0}{4\pi} \gamma_S \gamma_{j_k} \frac{3(\mathbf{n}_k \cdot \mathbf{S})(\mathbf{n}_k \cdot \mathbf{I}_k) - \mathbf{S} \cdot \mathbf{I}_k}{r_k^3 (1 + d/r_k)}, \quad (3)$$

$$h_3^k = \frac{\mu_0}{4\pi} \gamma_S \gamma_{j_k} \frac{\mathbf{L}_k \cdot \mathbf{I}_k}{r_k^3 (1 + d/r_k)}. \quad (4)$$

Here, $\gamma_S = 2\mu_B$, $\gamma_{j_k} = g_{j_k} \mu_N$, μ_B is the Bohr magneton, g_{j_k} is the nuclear g factor of isotopic species j_k , μ_N is the nuclear magneton, $\mathbf{r}_k = \mathbf{r} - \mathbf{R}_k$ is the electron-spin position operator relative to the nucleus, $d \approx Z \times 1.5 \times 10^{-15}$ m is a length of nuclear dimensions, Z is the charge of the nucleus, and $\mathbf{n}_k = \mathbf{r}_k / r_k$. \mathbf{S} and $\mathbf{L}_k = \mathbf{r}_k \times \mathbf{p}$ denote the spin and orbital angular-momentum operators of the electron, respectively.

Nuclear-spin interactions are typically much weaker than the spin-orbit interaction. It is therefore appropriate to form effective Hamiltonians with respect to a basis of eigenstates of the Coulomb and spin-orbit interactions. The 8×8 Kane Hamiltonian, which describes the band structure of a III–V semiconductor, provides such a basis.^{29,30} The Kane Hamiltonian is usually written in terms of conduction-band (CB) and valence-band [consisting of HH, light-hole (LH), and split-off sub-band] states. We derive an approximate basis of eigenstates in the HH sub-band by projecting the 8×8 Kane Hamiltonian onto the two-dimensional HH subspace.

To form effective Hamiltonians, we must approximate the crystal-Hamiltonian eigenfunctions given by Bloch's theorem for a single band n : $\Psi_{n\mathbf{k}\sigma}(\mathbf{r}) = \frac{1}{\sqrt{N_A}} e^{i\mathbf{k}\cdot\mathbf{r}} u_{n\mathbf{k}\sigma}(\mathbf{r})$, where N_A is the number of atomic sites in the crystal and the Bloch amplitudes $u_{n\mathbf{k}\sigma}(\mathbf{r})$ have the periodicity of the lattice.

We will approximate the $\mathbf{k}=\mathbf{0}$ Bloch amplitudes $u_{n\mathbf{0}\sigma}(\mathbf{r})$ within a primitive unit cell by a linear combination of atomic orbitals [see Eq. (12) below]. Near an atomic site, the CB Bloch amplitudes have approximate s symmetry (angular momentum $l=0$), whereas the HH and LH Bloch amplitudes have approximate p symmetry ($l=1$). Adding spin, the z component of total angular momentum of a HH is $m_j = \pm 3/2$, whereas a LH has $m_j = \pm 1/2$. In the Q2D limit, i.e., going from the bulk crystal to a quantum well (whose growth direction we take to be [001]), a splitting Δ_{LH} develops between the HH and LH sub-bands at $\mathbf{k}=\mathbf{0}$. We estimate $\Delta_{\text{LH}} \approx 100$ meV for a quantum well of height $a_z \approx 5$ nm in GaAs, much larger than the hyperfine coupling (see Appendix A). The splitting Δ_{LH} is essential since it produces a well-defined two-level system in the HH sub-band, and we can restrict our considerations to the manifold of $m_j = \pm 3/2$ states.

B. Interactions in an atom

Before addressing confinement in quantum dots, we illustrate that the interaction of an electron in a hydrogenic p orbital with the spin of the nucleus (which we choose to be at $\mathbf{R}_k=\mathbf{0}$) is generally nonzero. Moreover, when projected onto the manifold of $m_j = \pm 3/2$ states, this interaction takes on a simple Ising form. Although our final analysis will apply to any III–V semiconductor, we will take GaAs as a concrete example.

The effective screened nuclear charges Z_{eff} “felt” by the valence electrons (in $4s$ and $4p$ orbitals) in Ga and As atoms have been calculated in Ref. 31. The $4s$ orbitals and $4p$ orbitals (with orbital angular momentum $m_L = \pm 1$) are given in terms of hydrogenic eigenfunctions with the replacements

$Z \rightarrow Z_{\text{eff}}$ by $\Psi_{400}(\mathbf{r}) = R_{40}(r) Y_0^0(\theta, \varphi)$ and $\Psi_{41\pm 1}(\mathbf{r}) = R_{41}(r) Y_1^{\pm 1}(\theta, \varphi)$, respectively. Including spin and evaluating matrix elements of the Hamiltonians (2)–(4) with respect to hydrogenic $4s$ states leads to effective spin Hamiltonians of the form^{28,32} $h_1^{4s} = A_s \mathbf{S} \cdot \mathbf{I}_k$ and, due to the spherical symmetry of the wave function, $h_2^{4s} = h_3^{4s} = 0$. The same procedure with the $4p$ states leads to effective Hamiltonians $h_1^{4p} = 0$ (since p states vanish at the origin) and $h_2^{4p} + h_3^{4p} = A_p s_z I_k^z$, where $s_z = \pm \frac{1}{2}$ corresponds to $m_j = \pm 3/2$. A_s and A_p denote the coupling strengths of electrons in $4s$ and $4p$ orbitals, respectively. Evaluating all integrals exactly gives

$$\frac{A_p}{A_s} = \frac{1}{5} \left(\frac{Z_{\text{eff}}(\kappa, 4p)}{Z_{\text{eff}}(\kappa, 4s)} \right)^3, \quad \kappa = \text{Ga, As}. \quad (5)$$

Quite significantly, after inserting values of Z_{eff} from Ref. 31 into Eq. (5), we find that the ratio of coupling strengths is fairly large—of order 10%: $A_p/A_s \approx 0.14$ for Ga and $A_p/A_s \approx 0.11$ for As. Since h_2^k and h_3^k do not contribute to the hyperfine interaction of an electron in an s orbital, research on hyperfine interaction for electrons in an s -type conduction band has focused on the contact term h_1^k , neglecting the other interactions. The fact that h_1^k , in contrast, gives no contribution for an electron in a p orbital has led to the claim that electrons in p orbitals (and holes) do not interact with nuclear spins. Equation (5) shows that h_2^k and h_3^k can contribute significantly. Furthermore, while the interaction of a $4s$ electron with the nuclear spin is of Heisenberg type, within the manifold of $m_j = \pm 3/2$ states, the interaction of a $4p$ electron is Ising at leading order (virtual transitions via the $m_j = \pm 1/2$ states may lead to non-Ising corrections). This result is a direct consequence of the Wigner-Eckart theorem and the fact that the Hamiltonians (2)–(4) can be written in the form $h_i^k = \mathbf{v}_i^k \cdot \mathbf{I}_k$, where \mathbf{v}_i^k are vector operators in the electron (spin and orbital) Hilbert space.

C. Interactions in a quantum dot

We now return to the problem directly relevant to a HH in a two-dimensional quantum well. We consider an additional circular-symmetric parabolic confining potential in the plane of the quantum well defining a quantum dot. Neglecting hybridization with other bands, which we estimate to be typically of order 1% (see Appendix A), the pseudospin states for a HH within the envelope-function approximation read $|\Psi_{\sigma}\rangle = |\phi; u_{\text{HH0}\sigma}\rangle |\sigma\rangle$, where $|\phi; u_{\text{HH0}\sigma}\rangle$ and $|\sigma\rangle$ ($\sigma = \pm$) denote the orbital and spin states, respectively. The orbital wave functions are given explicitly by $\langle \mathbf{r} | \phi; u_{\text{HH0}\sigma}\rangle = \sqrt{v_0} \phi(\mathbf{r}) u_{\text{HH0}\sigma}(\mathbf{r})$. Here, v_0 is the volume occupied by a single atom (half the volume of a two-atom zinc-blende primitive unit cell) and $\phi(\mathbf{r}) = \phi_z(z) \phi_\rho(\rho)$ is the envelope function. The radial ground-state envelope function is a Gaussian

$$\phi_\rho(\rho) = \frac{1}{\sqrt{\pi} l} \exp\left(-\frac{\rho^2}{2l^2}\right), \quad (6)$$

where $\boldsymbol{\rho} = (x, y)$, $\rho = |\boldsymbol{\rho}|$, $l = l_0 [1 + (B_z/B_0)^2]^{-1/4}$, B_z is the component of an externally applied magnetic field along the growth direction, and $B_0 = \Phi_0 / \pi l_0^2$, where $\Phi_0 = h/e|e|$ is a flux

TABLE I. Estimates of the coupling strengths for a HH (A_h^j) and a CB electron (A_e^j) for the three isotopes in GaAs. Columns (i) and (iii) show values obtained from a linear combination of hydrogenic eigenfunctions using free-atom values of Z_{eff} calculated in Ref. 31. Column (iv) gives the accepted values of A_e^j from Ref. 35. Column (ii) shows the rescaled values from column (i) (see text). In the last row we give the average coupling constants weighted by the natural isotopic abundances $\nu^{69\text{Ga}}=0.3$, $\nu^{71\text{Ga}}=0.2$, and $\nu^{75\text{As}}=0.5$.

j	A_h^j (μeV)		A_e^j (μeV)	
	(i)	(ii)	(iii)	(iv)
^{69}Ga	-7.1	-13	40	74
^{71}Ga	-9.0	-17	51	94
^{75}As	-8.2	-12	59	89
$A_\alpha = \sum_j \nu_j A_\alpha^j$ ($\alpha = e, h$)	-8.0	-13	52	86

quantum. A typical dot Bohr radius of $l_0=30$ nm gives $B_0 \approx 1.5$ T.

In a solid, the HH is delocalized over the lattice sites of the crystal. The nuclei do not interact solely with the fraction of the HH in the same primitive unit cell (“on-site” interaction), but also with density localized at more distant atomic sites (long-ranged interactions). We neglect the long-ranged interactions, which lead to corrections of order 1% relative to the on-site interaction (see Appendix C). If the envelope function varies slowly on the length scale of a primitive cell, we find (combining h_2^k and h_3^k): $A_h^k = A_h^k v_0 |\phi(\mathbf{R}_k)|^2$, where

$$A_h^k = -\frac{\mu_0}{4\pi} \gamma_S \gamma_{j_k} \left\langle \frac{3 \cos^2 \theta_k + 1}{r_k^3 (1 + d/r_k)} \right\rangle_{\text{p.c.}}. \quad (7)$$

Here, $\langle \dots \rangle_{\text{p.c.}}$ denotes the expectation value with respect to $u_{\text{HH}0\sigma}(\mathbf{r})$ over a primitive unit cell ($\sigma = \pm$ give the same matrix elements) and θ_k is the polar angle of \mathbf{r}_k . The magnetic moment of a HH is inverted with respect to that for an electron. This results in a change of sign in Eqs. (2)–(4) and leads to the minus sign in Eq. (7) and of the values in columns (i) and (ii) of Table I.

D. Non-Ising corrections

There will be small corrections to the form of the effective Hamiltonian given in Eq. (1). Evaluating off-diagonal matrix elements of Eqs. (3) and (4) with the approximate Bloch amplitudes (12) yields non-Ising terms, whose associated coupling strengths A_h^\perp we find to be small ($A_h^\perp < 0.06 A_h^j$). Higher-order virtual transitions between the $m_j = \pm 3/2$ states via the LH sub-band are suppressed by $\sim A_h^h / \Delta_{\text{LH}} \ll 1$. Hybridization with other bands can also lead to non-Ising corrections. For unstrained quantum dots, we find that these corrections are small, typically of order 1% of the values given in Table I (see also Appendix A). Strain can lead to considerably stronger band mixing and, hence, to significantly larger non-Ising corrections to Eq. (1).

III. SPIN DECOHERENCE

Now that the effective Hamiltonian [Eq. (1)] has been established, we can analyze the dephasing of a HH pseudospin in the presence of a random nuclear environment. In an applied magnetic field, pseudospin dynamics of the HH are described by the Hamiltonian

$$H = (b_\perp + h_z) s_z + b_\parallel s_x, \quad (8)$$

where $h_z = \sum_k A_k^h I_k^z$ is the nuclear field operator, $b_\perp = g_\perp \mu_B B_z$ is the Zeeman splitting due to a magnetic field B_z along the growth direction, and $b_\parallel = g_\parallel \mu_B B_x$ is the Zeeman splitting due to an applied magnetic field B_x in the plane of the quantum dot. g_\perp and g_\parallel are the components of the HH g tensor along the growth direction and in the plane of the quantum dot, respectively (we assume the in-plane g tensor to be isotropic).

If no special effort is made to control the nuclear field, the field value will be Gaussian-distributed in the limit of a large number of nuclear spins.⁶ The variance for a random nuclear-spin distribution is (see Appendix D)

$$\langle h_z^2 \rangle = \sigma^2 \approx \frac{1}{4N} \sum_j \nu_j j(j+1) (A_h^j)^2, \quad (9)$$

where $N = \pi l^2 a_z / v_0$ is the number of nuclei within the quantum dot. The nuclear-field fluctuation σ therefore inherits a magnetic-field dependence from l [see Eq. (6)]. A finite nuclear-field variance will result in a random distribution of precession frequencies experienced by the hole pseudospin inducing pure dephasing (decay of the components of hole pseudospin transverse to \mathbf{B}).

First, we consider the case $b_\parallel = 0$. For a hole pseudospin initially oriented along the x direction, we find a Gaussian decay [see Fig. 1(a)] of the transverse pseudospin in the rotating frame $\langle \tilde{s}_+ \rangle_t = \exp(-ib_\perp t) (\langle s_x \rangle_t + i \langle s_y \rangle_t)$:

$$\langle \tilde{s}_+ \rangle_t = \frac{1}{2} \exp\left(-\frac{t^2}{2\tau_\perp^2}\right), \quad \tau_\perp = \frac{1}{\sigma}. \quad (10)$$

This is the same Gaussian decay that occurs for electrons.^{4–6} Here, since the magnetic field is taken to be out of plane, we must take account of the diamagnetic “squeezing” of the wave function. This squeezing affects the number N of nuclear spins within the dot and hence, the finite-size fluctuation σ . The coherence time $\tau_\perp(B_z) = 1/\sigma(B_z) = \tau_\perp(0) [1 + (B_z/B_0)^2]^{-1/4}$ then *decreases* for large B_z [see Fig. 1(b)]. This undesirable effect can be avoided for confined electron spins by generating a large Zeeman splitting through an in-plane (rather than out-of-plane) magnetic field. This option may not be available for a HH where, typically, $g_\parallel \ll g_\perp$.

The situation changes drastically for an in-plane magnetic field ($b_\perp = 0$). In this case, since the hyperfine fluctuations are purely transverse to the applied field direction, the decay is given by a slow power law at long times [see Fig. 1(c)] and the relevant dephasing time *increases* as a function of the applied magnetic field [see Fig. 1(d)]. In the limit $b_\parallel \gg \sigma$ and for a HH pseudospin initially prepared along the \hat{z} direction, we find

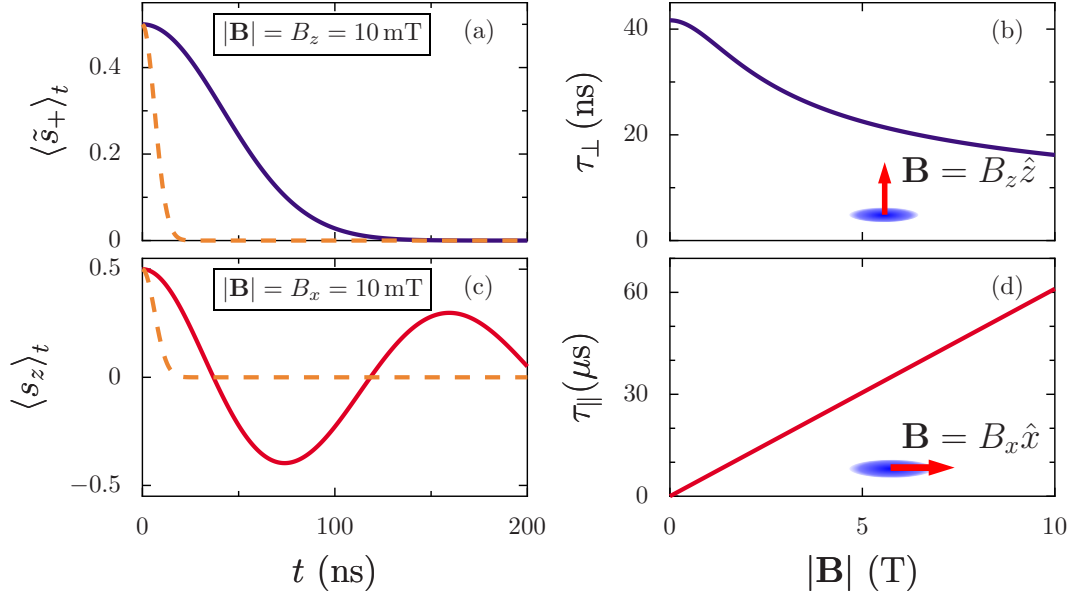


FIG. 1. (Color online) Dephasing of HH pseudospin states [solid lines in (a) and (c)]. The decay is Gaussian for (a) an out-of-plane magnetic field B_z [see Eq. (10)] and given by a slow power law at long times ($\sim 1/\sqrt{t}$) for (c) an in-plane magnetic field B_x [see Eq. (11)]. We have chosen $|\mathbf{B}|=10$ mT in (a) and (c). Magnetic-field dependences of the relevant coherence times are shown for a field that is (b) out-of-plane and (d) in-plane. We have assumed $g_{\parallel}=0.04$ (from Ref. 33) and a zero-field lateral dot size $l_0=30$ nm and height $a_z=5$ nm, leading to $N=\pi l_0^2 a_z/v_0=6.5 \times 10^5$ nuclei within the dot at $B_z=0$. We have taken $v_0=a_L^3/8$, where $a_L=5.65$ Å is the GaAs lattice constant. The dashed lines in (a) and (c) show the dephasing of CB electron-spin states in the high-field limit $|\mathbf{B}| \gg \sigma_e/g_e \mu_B$, where g_e is the electron g factor and σ_e is obtained from Eq. (9) by replacing A_h^j by the electron hyperfine coupling constants A_e^j .

$$\langle s_z \rangle_t \approx \frac{\cos(b_{\parallel}t + \frac{1}{2}\arctan(t/\tau_{\parallel}))}{2[1 + (\frac{t}{\tau_{\parallel}})^2]^{1/4}}, \quad \tau_{\parallel} = \frac{b_{\parallel}}{\sigma^2}. \quad (11)$$

The derivation of Eq. (11) is directly analogous to that for the decay of driven Rabi oscillations in Ref. 34.

IV. ESTIMATES OF THE COUPLING STRENGTHS

To estimate the size of A_h^j , we need an explicit expression for the HH $\mathbf{k}=\mathbf{0}$ Bloch amplitudes. We approximate $u_{\text{HH}0\sigma}(\mathbf{r})$ within a Wigner-Seitz cell centered halfway along the Ga-As bond by a linear combination of atomic orbitals, following Ref. 36:

$$u_{\text{HH}0\sigma}(\mathbf{r})|_{\mathbf{r} \in \text{WS}} = N_{\alpha_v} [\alpha_v \Psi_{41\sigma}^{\text{Ga}}(\mathbf{r} + \mathbf{d}/2) + \sqrt{1 - \alpha_v^2} \Psi_{41\sigma}^{\text{As}}(\mathbf{r} - \mathbf{d}/2)]. \quad (12)$$

Here, $\mathbf{d} = \frac{a}{4}(1, 1, 1)$ is the Ga-As bond vector, a is the lattice constant, α_v describes the relative electron sharing at the Ga and As sites in the HH sub-band, and N_{α_v} is a normalization constant, chosen to enforce $\int_{\text{WS}} d^3r |u_{\text{HH}0\sigma}(\mathbf{r})|^2 = 2$, where the integration is performed over the Wigner-Seitz cell defined above. To simplify numerical integration, we replace the Wigner-Seitz cell by a sphere centered halfway along the Ga-As bond, with radius given by half the Ga-Ga nearest-neighbor distance. We find the electron sharing in the CB from the densities given in Ref. 35 to be $\alpha_c^2 \approx 1/2$ (see Appendix B) and assume the same ($\alpha_v^2 = 1/2$) for Eq. (12). Using Z_{eff} for free atoms,³¹ we evaluate Eq. (7) with the ansatz, Eq. (12), by numerical integration, giving the values shown

in Table I, column (i). We check the validity of this procedure by writing the CB Bloch amplitudes as in Eq. (12), replacing the $4p$ eigenfunctions by $4s$ eigenfunctions. Evaluating the coupling constants for the CB (A_e^j) from h_1^k gives the numbers in column (iii). The accepted values of A_e^j from Ref. 35 are shown in column (iv) for comparison. Our method produces A_e^j to within a factor of two of the accepted values. Our procedure, which relies on free-atom orbitals, most likely underestimates the electron density near the atomic sites, which should be enhanced in a solid due to confinement. Assuming the relative change in density going from a free atom to a solid is the same for the CB and HH band, we rescale the results in column (i) by the ratio of the values in columns (iv) and (iii), giving column (ii). Due to the approximations involved, we expect the values in columns (i) and (ii) only to be valid to within a factor of 2 or 3.

V. CONCLUSIONS

We have shown that the interaction of a quantum-dot-confined heavy hole with nuclear spins is stronger than previously anticipated. We have estimated the associated coupling strength to be of order 10 μeV in GaAs—only 1 order of magnitude less than the hyperfine coupling for electrons. However, the interaction turns out to be Ising which has profound consequences for hole-spin decoherence. Since no flip-flop terms occur in the effective Hamiltonian [Eq. (1)], the main source of decoherence is given by the broad frequency distribution of the nuclear spins. Recent theoretical and experimental studies have shown that state-narrowing techniques are capable of strongly suppressing this source of

decoherence, which makes the heavy hole an attractive spin-qubit candidate.

Very recently, experimental results on hole-spin relaxation in self-assembled quantum dots have been released.^{9,11} Gerardot *et al.* reported an extremely weak coupling of HH spin states, which is explained by our theory to be a direct consequence of the Ising-type nuclear-spin interaction (negligible flip-flop terms). Eble *et al.*, in contrast, found very short hole-spin relaxation times in order of 15 ns. This is due to the strong strain present in the particular dots used in this experiment, resulting in a considerable HH-LH mixing and a highly non-Ising interaction (large flip-flop terms).

ACKNOWLEDGMENTS

We acknowledge discussions with S. I. Erlingsson and D. Stepanenko and funding from the Swiss NSF, NCCR Nanoscience, JST ICORP, QuantumWorks, an Ontario PDF (WAC), and the “Dynasty” Foundation (DVB).

APPENDIX A: HEAVY-HOLE STATES

In this section we give details on our derivation of an approximate basis of heavy-hole eigenstates in a quantum dot. We will approximate the ground-state quantum-dot envelope function in the HH sub-band by

$$\phi(\mathbf{r}) = \phi_z(z)\phi_\rho(\rho), \quad (\text{A1})$$

$$\phi_\rho(\rho) = \frac{1}{\sqrt{\pi}l} \exp\left(-\frac{\rho^2}{2l^2}\right), \quad (\text{A2})$$

$$\phi_z(z) = \sqrt{\frac{2}{a_z}} \sin\left(\frac{\pi z}{a_z}\right), \quad z = [0 \dots a_z], \quad (\text{A3})$$

where a_z is the width of the confinement potential along the growth direction [for definition of the other symbols see Eq. (6)]. We will then estimate the size of the splitting Δ_{LH} between the HH and the light-hole band and the degree of hybridization with the conduction band, LH, and split-off (SO) sub-bands.

We start from the 8×8 Kane Hamiltonian given in Ref. 37 for bulk zinc-blende-type crystals, which is written in terms of the exact eigenstates (near $\mathbf{k}=\mathbf{0}$) of an electron in the CB, HH, LH, and SO bands, usually denoted by $|1/2; \pm 1/2\rangle_c$, $|3/2; \pm 3/2\rangle_v$, $|3/2; \pm 1/2\rangle_v$, and $|1/2; \pm 1/2\rangle_v$, respectively. We neglect terms that are more than 2 orders of magnitude smaller than the fundamental band-gap energy E_g ⁴⁰ and perform the quasi-two-dimensional limit by assuming that a confinement potential has been applied along the growth direction. If the confinement potential is sufficiently strong (i.e., if the quantum well is sufficiently narrow), the energy-level spacing will be large and the electron will be in the ground state at low temperatures. Any operator acting on the z component of the electron envelope function can then be replaced by its expectation value with respect to the z component of the ground-state envelope function. For the Kane Hamiltonian this means that we can replace powers of the z component $\hbar k_z$ of the crystal

momentum $\hbar \mathbf{k}$ by expectation values. Assuming an infinite square-well potential of width a_z confining the electron along the growth direction, the ground state is given by Eq. (A3). Calculating the expectation value of k_z and k_z^2 with respect to the ground state, we find $\langle k_z \rangle = 0$ and $\langle k_z^2 \rangle = \pi^2/a_z^2$. This allows us to write the Kane Hamiltonian in the following form:

$$H_K = \begin{pmatrix} H_{\text{CB}} & V_1 & V_2 & V_3 \\ V_1^\dagger & H_{\text{HH}} & V_4 & V_5 \\ V_2^\dagger & V_4^\dagger & H_{\text{LH}} & V_6 \\ V_3^\dagger & V_5^\dagger & V_6^\dagger & H_{\text{SO}} \end{pmatrix}, \quad (\text{A4})$$

where

$$H_{\text{CB}} = \begin{pmatrix} A & 0 \\ 0 & A \end{pmatrix}, \quad H_{\text{HH}} = \begin{pmatrix} B & 0 \\ 0 & B \end{pmatrix},$$

$$H_{\text{LH}} = \begin{pmatrix} C & 0 \\ 0 & C \end{pmatrix}, \quad H_{\text{SO}} = \begin{pmatrix} D & 0 \\ 0 & D \end{pmatrix},$$

$$V_1 = \frac{1}{\sqrt{2}} \begin{pmatrix} -E & 0 \\ 0 & E^* \end{pmatrix}, \quad V_2 = \frac{1}{\sqrt{6}} \begin{pmatrix} 0 & E^* \\ -E & 0 \end{pmatrix},$$

$$V_3 = \frac{1}{\sqrt{3}} \begin{pmatrix} 0 & -E^* \\ -E & 0 \end{pmatrix}, \quad V_4 = \sqrt{3} \begin{pmatrix} 0 & F \\ F^* & 0 \end{pmatrix},$$

$$V_5 = \sqrt{6} \begin{pmatrix} 0 & -F \\ F^* & 0 \end{pmatrix}, \quad V_6 = \sqrt{2} \begin{pmatrix} -G & 0 \\ 0 & G \end{pmatrix},$$

and

$$A = E_g + \hbar^2(k_x^2 + k_y^2 + \langle k_z^2 \rangle)/2m',$$

$$B = -\epsilon[(\gamma'_1 + \gamma'_2)(k_x^2 + k_y^2) + (\gamma'_1 - 2\gamma'_2)\langle k_z^2 \rangle],$$

$$C = -\epsilon[(\gamma'_1 - \gamma'_2)(k_x^2 + k_y^2) + (\gamma'_1 + 2\gamma'_2)\langle k_z^2 \rangle],$$

$$D = -\epsilon\gamma'_1(k_x^2 + k_y^2 + \langle k_z^2 \rangle) - \Delta_{\text{SO}},$$

$$E = Pk_+,$$

$$F = \epsilon[\gamma'_2(k_x^2 - k_y^2) - 2i\gamma'_3k_xk_y],$$

$$G = \epsilon\gamma'_2(k_x^2 + k_y^2 - 2\langle k_z^2 \rangle).$$

Here, $\epsilon = \hbar^2/2m_0$ and m_0 is the free-electron mass, whereas m' is the effective mass of a CB electron. Furthermore, $k_\pm = k_x \pm ik_y$, γ'_j denote the Luttinger parameters, P is the inter-band momentum, and Δ_{SO} is the spin-orbit gap between the LH and the SO bands. Experimental values for these parameters can be found in Table II.

We assume a circular-symmetric parabolic confinement potential with frequency ω_0 in the xy plane defining a quantum dot. Including a magnetic field along the growth direction, the ground state is approximately described by the Gaussian given in Eq. (A2). The envelope function of the quantum dot is then the product of the in-plane and out-of-plane components as given in Eq. (A1).

TABLE II. Values of band parameters used in Appendix A.

P (eV Å)	10.5 ^a	γ'_1	6.98 ^b
E_g (eV)	1.52 ^a	γ'_2	2.06 ^b
Δ_{SO} (eV)	0.34 ^a	γ'_3	2.93 ^b

^aTaken from Ref. 37.^bTaken from Ref. 38.

In the quasi-two-dimensional limit, a gap

$$\Delta_{\text{LH}} = \langle B - C \rangle = -\frac{\hbar^2 \gamma'_2}{m_0} (\langle k_x^2 \rangle + \langle k_y^2 \rangle - 2\langle k_z^2 \rangle) \quad (\text{A5})$$

develops between the HH and LH sub-bands, lifting the HH-LH degeneracy. Here, $\langle \dots \rangle$ denotes the expectation value with respect to the envelope function given in Eq. (A1). The in-plane level spacing scales like $\sim 1/l^2$, where l is the dot Bohr radius. The in-plane level spacing is much smaller than the level spacing along the growth direction since, for typical dots, $a_z^2 \ll l^2$. Neglecting $\langle k_x^2 \rangle$ and $\langle k_y^2 \rangle$ compared to $\langle k_z^2 \rangle$ in Eq. (A5) and inserting $\langle k_z^2 \rangle = \pi^2/a_z^2$ for a square-well potential, we estimate

$$\Delta_{\text{LH}} \approx \frac{2\pi^2 \gamma'_2 \hbar^2}{a_z^2 m_0} \approx 100 \text{ meV} \quad (\text{A6})$$

for $a_z \approx 5$ nm, using $\gamma'_2 \approx 2.06$ for GaAs (see Table II). The HH-LH splitting is thus much larger than the typical energy scale associated with the hyperfine interaction ($A_e \approx 90 \mu\text{eV}$ for CB electrons in GaAs).

To derive the approximate electron eigenfunctions in the HH sub-band of the quantum well, we start from the Kane Hamiltonian (A4). We use quasidegenerate perturbation theory up to first order in $1/\mathcal{E}$ (where \mathcal{E} stands for E_g , Δ_{LH} , or $\Delta_{\text{LH}} + \Delta_{\text{SO}}$), taking H_{HH} as the unperturbed Hamiltonian.³⁷ This leads to a band-hybridized state of the form

$$|\Psi_{\text{HH,hyb}}^\sigma\rangle = \mathcal{N}_\sigma \sum_n \lambda_n^\sigma |\phi_{n\sigma}; u_{n0\sigma}\rangle. \quad (\text{A7})$$

Here, $\sigma = \pm$, $\langle \mathbf{r} | \phi_{n\sigma}; u_{n0\sigma} \rangle = \sqrt{v_0} \phi_{n\sigma}(\mathbf{r}) u_{n0\sigma}(\mathbf{r})$ is the product of envelope function, and $\mathbf{k} = \mathbf{0}$ Bloch amplitude in band n (CB, HH, LH, or SO), the prefactors λ_n^σ describe the degree of band hybridization, and \mathcal{N}_σ enforces proper normalization.

In first-order quasidegenerate perturbation theory, the hybridization with the CB and the LH and SO sub-bands is described by the interaction terms V_1 , V_4 , and V_5 in Eq. (A4), respectively. We estimate the degree of hybridization by applying these operators to a two-spinor containing the in-plane ground-state envelope function (A2) of the HH sub-band. For the hybridization with the conduction band, we find (for $\mathbf{B} = \mathbf{0}$)

$$-\frac{1}{E_g} V_1 \begin{pmatrix} \phi_\rho(\rho) \\ \phi_\rho(\rho) \end{pmatrix} = \begin{pmatrix} \lambda_{\text{CB}}^+ \phi_{\text{CB}\rho^+}(\rho) \\ \lambda_{\text{CB}}^- \phi_{\text{CB}\rho^-}(\rho) \end{pmatrix}, \quad (\text{A8})$$

where

$$\phi_{\text{CB}\rho^\pm}(\rho) = \frac{i}{\sqrt{2}} [\psi_{10}(\rho) \pm i\psi_{01}(\rho)]. \quad (\text{A9})$$

Here, $\psi_{nm}(\rho) = \psi_n(x)\psi_m(y)$ and $\psi_n(x)$ is the n th harmonic-oscillator eigenstate. The envelope function of the admixed CB state is a superposition of *excited* harmonic-oscillator eigenfunctions. The prefactor

$$\lambda_{\text{CB}}^\pm = \pm \frac{P}{\sqrt{2}E_g l_0} \quad (\text{A10})$$

determines the degree of sp hybridization. Using values from Table II and assuming a quantum dot with dot Bohr radius $l_0 \approx 30$ nm ($\mathbf{B} = \mathbf{0}$), we estimate $\lambda_{\text{CB}}^\pm \approx 10^{-2}$. Similarly, we estimate $\lambda_{\text{LH}}^\pm \approx \lambda_{\text{SO}}^\pm \approx 10^{-3}$, assuming a dot height $a_z \approx 5$ nm. The admixture of CB, LH, and SO states to the HH state is thus in order of 1% and has therefore been neglected in our considerations.

We emphasize that sp hybridization will lead to a coupling of the HH to the nuclear spins via the Fermi contact interaction (2). Since the Fermi contact interaction is of Heisenberg type, sp hybridization will directly lead to non-Ising corrections to the effective Hamiltonian given in Eq. (1). The size of these corrections is determined by the degree of sp hybridization which is of order 1% (see above).

APPENDIX B: ESTIMATE OF THE FERMI CONTACT INTERACTION

In Eq. (12), we have approximated the HH $\mathbf{k} = \mathbf{0}$ Bloch amplitudes within a Wigner-Seitz cell by a linear combination of atomic orbitals. Similarly, we approximate the $\mathbf{k} = \mathbf{0}$ Bloch amplitude in the CB by

$$u_{\text{CB0}\sigma}(\mathbf{r})|_{\mathbf{r} \in \text{WS}} = N_{\alpha_c} [\alpha_c \Psi_{400}^{\text{Ga}}(\mathbf{r} + \mathbf{d}/2) - \sqrt{1 - \alpha_c^2} \Psi_{400}^{\text{As}}(\mathbf{r} - \mathbf{d}/2)], \quad (\text{B1})$$

independent of σ . Here, $\Psi_{400}(\mathbf{r}) = R_{40}(r)Y_0^0(\theta, \varphi)$, α_c describes the relative electron sharing between the Ga and As atom in the Wigner-Seitz cell chosen to be centered halfway along the Ga-As bond, and N_{α_c} normalizes the Bloch amplitude to two atoms in a primitive unit cell. The radial wave function depends implicitly on the effective nuclear charges $Z_{\text{eff}}(\kappa, 4s)$, where $\kappa = \text{Ga, As}$.

We will estimate the relative electron sharing in the CB by calculating the electron densities at the sites of the nuclei from Eq. (B1) and comparing to accepted values taken from Ref. 35. We will then estimate the Fermi contact interaction of a CB electron using free-atom effective nuclear charges taken from Ref. 31 [$Z_{\text{eff}}(\text{Ga}, 4s) \approx 7.1$, $Z_{\text{eff}}(\text{Ga}, 4p) \approx 6.2$, $Z_{\text{eff}}(\text{As}, 4s) \approx 8.9$, and $Z_{\text{eff}}(\text{As}, 4p) \approx 7.4$] and normalizing the Bloch amplitude over a Wigner-Seitz cell.

We approximate the electron densities at the Ga and As sites within a primitive unit cell from Eq. (B1)

$$d_{\text{Ga}} = |u_{\text{CB0}\sigma}(-\mathbf{d}/2)|^2 \approx N_{\alpha_c}^2 \alpha_c^2 |\Psi_{400}^{\text{Ga}}(0)|^2, \quad (\text{B2})$$

$$d_{\text{As}} = |u_{\text{CB0}\sigma}(\mathbf{d}/2)|^2 \approx N_{\alpha_c}^2 (1 - \alpha_c^2) |\Psi_{400}^{\text{As}}(0)|^2. \quad (\text{B3})$$

We estimate the corrections to the right-hand sides to be of order 1% due to overlap terms. We take the ratio $d_{\text{Ga}}/d_{\text{As}}$ and

equate this with the ratio of the values from Ref. 35, $d'_{\text{Ga}} = 5.8 \times 10^{-31} \text{ m}^{-3}$ and $d'_{\text{As}} = 9.8 \times 10^{-31} \text{ m}^{-3}$. This allows us to write α_c as a function of the two effective nuclear charges

$$\alpha_c = \left[1 + \frac{d_{\text{As}}}{d_{\text{Ga}}} \left(\frac{Z_{\text{eff}}(\text{Ga}, 4s)}{Z_{\text{eff}}(\text{As}, 4s)} \right)^3 \right]^{-1/2}. \quad (\text{B4})$$

Recalling that N_{α_c} normalizes the Bloch amplitude to two atoms over a Wigner-Seitz cell, we write

$$N_{\alpha_c} = \left[\frac{1}{2} \int_{\text{WS}} d^3r |\alpha_c \Psi_{400}^{\text{Ga}}(\mathbf{r} + \mathbf{d}/2) - \sqrt{1 - \alpha_c^2} \Psi_{400}^{\text{As}}(\mathbf{r} - \mathbf{d}/2)|^2 \right]^{-1/2}. \quad (\text{B5})$$

For all numerical integrations, we approximate the Wigner-Seitz cell by a sphere centered halfway along the Ga-As bond with radius equal to half the Ga-Ga nearest-neighbor distance. Inserting (B4) and (B5) into (B2) and (B3), we solve the two coupled equations

$$d_{\text{Ga}}[Z_{\text{eff}}(\text{Ga}), Z_{\text{eff}}(\text{As})] - d'_{\text{Ga}} = 0, \quad (\text{B6})$$

$$d_{\text{As}}[Z_{\text{eff}}(\text{Ga}), Z_{\text{eff}}(\text{As})] - d'_{\text{As}} = 0, \quad (\text{B7})$$

for the two effective nuclear charges. This yields $Z_{\text{eff}}(\text{Ga}) \approx 9.8$ and $Z_{\text{eff}}(\text{As}) \approx 11.0$. Inserting these values back into Eq. (B4), we estimate the electron sharing within the primitive unit cell to be

$$\alpha_c^2 \approx 0.46. \quad (\text{B8})$$

For comparison, inserting free-atom effective nuclear charges into Eq. (B4) yields a similar value ($\alpha_c^2 \approx 0.54$).

Now we estimate the Fermi contact interaction of a CB electron starting from the free-atom effective nuclear charges $Z_{\text{eff}}(\kappa, 4s)$ obtained from Ref. 31. We use $\alpha_c \approx 1/\sqrt{2}$ and normalize the $\mathbf{k}=\mathbf{0}$ Bloch amplitude to two atoms over a Wigner-Seitz cell, following Eq. (B5). From the normalized Bloch amplitudes we estimate the Fermi contact hyperfine interaction by evaluating

$$A_e^j = \frac{2\mu_0}{3} \gamma_S \gamma_j |u_{\text{CB}0\sigma}(\mathbf{R}_j)|^2. \quad (\text{B9})$$

Here, $\mathbf{R}_j = \mp \mathbf{d}/2$ for Ga and As, respectively (j indexes the nuclear isotope). Evaluating for the isotopes in GaAs, this gives the values shown in column (iii) of Table I.

Replacing the Wigner-Seitz cell by a sphere with radius R_s equal to half the Ga-Ga nearest-neighbor distance in our numerical integrations overestimates the expectation value of $[r_k^3(1+d/r_k)]^{-1}$ in Eq. (7). To estimate the error, we perform an integration over a sphere with radius $R'_s = (R_s + R_{\text{max}})/2$, where R_{max} denotes the radius of the smallest sphere that fully contains the Wigner-Seitz cell. From this, we estimate the relative error to be less than 30%.

APPENDIX C: ESTIMATE OF THE LONG-RANGED INTERACTIONS

In this section, we estimate the corrections to the HH coupling strength in Eq. (7) due to long-ranged dipole-dipole

interactions and long-ranged $\mathbf{L} \cdot \mathbf{I}$ interactions. To this end, we consider a single nucleus interacting with a HH that is delocalized over the lattice sites in the quantum dot. We start from the Hamiltonians given in Eqs. (3) and (4). We define effective radii $a_{\text{eff}}(\kappa, 4p) = a_0/Z_{\text{eff}}(\kappa, 4p)$, where $a_0 \approx 5.3 \times 10^{-11} \text{ m}$ is the Bohr radius. The effective radii define an approximate length scale for the spread of the site-localized functions $\Psi_{41\sigma}^{\kappa}(\mathbf{r})$ and are much smaller than the GaAs lattice constant $a_L \approx 5.7 \times 10^{-10} \text{ m}$. The nucleus thus effectively “sees” sharp-peaked electron densities centered around the more distant lattice sites. We choose the nucleus to be at site \mathbf{R}_k and estimate the interaction with the electron density at more distant atomic sites by approximating the electron densities by δ functions. Adding up contributions from h_2^k and h_3^k , we arrive at an effective Hamiltonian describing the long-ranged interactions: $H_{\text{lr}}^k = A_{\text{lr}}^k S_z I_k^z$, where $A_{\text{lr}}^k = \sum_{l,l \neq k} A_{\text{lr}}^{kl}$ is the associated coupling strength and $A_{\text{lr}}^{kl} = v_0 |\phi(\mathbf{R}_l)|^2 \int d^3r_k \delta(\mathbf{r}_k - \mathbf{R}_{kl}) (h_2^k + h_3^k)$ describes the coupling of the electron density at site \mathbf{R}_l to the nucleus at site \mathbf{R}_k ($\mathbf{R}_{kl} = \mathbf{R}_l - \mathbf{R}_k$). In order to estimate the size of the long-ranged interactions relative to the on-site interactions, we take into account nearest-neighbor couplings for the long-ranged part, i.e., we replace $\sum_{l,l \neq k} \rightarrow \sum_{l=\text{n.n.}}$. The interaction with electron density located around more distant nuclei is suppressed by $\sim 1/R_{kl}^3$. Assuming that the quantum-dot envelope function varies slowly over the nearest-neighbor distance [$\phi(\mathbf{R}_l) \approx \phi(\mathbf{R}_k)$ for l nearest neighbor of k], we estimate the ratio of long-ranged and on-site interactions [Table I column (i)] to be

$$\frac{A_{\text{lr}}}{A_h} \approx 7 \times 10^{-3}, \quad (\text{C1})$$

of order 1%, where $A_{\text{lr}}^k = A_{\text{lr}} v_0 |\phi(\mathbf{R}_k)|^2$.

We remark that, in principle, the electron g factor can deviate from the free-electron g factor due to spin-orbit interaction. According to Ref. 39, this renormalization is negligible for the on-site interaction, but could become relevant for the long-ranged interaction. However, for the estimate in Eq. (C1), we have taken the free-electron g factor.

APPENDIX D: VARIANCE OF THE NUCLEAR FIELD

Here we calculate the nuclear-field variance for a HH interacting with nuclei in a quantum dot. In particular, we evaluate

$$\sigma^2 = \langle h_z^2 \rangle, \quad (\text{D1})$$

where $\langle \dots \rangle = \text{Tr}_I(\bar{\rho}_I \dots)$ indicates the expectation value with respect to the infinite-temperature thermal equilibrium density matrix $\bar{\rho}_I$ and we recall $h_z = \sum_k A_k^h I_k^z$. For an uncorrelated and unpolarized nuclear state, we have $\langle I_k^z I_{k'}^z \rangle = \langle I_k^z \rangle \langle I_{k'}^z \rangle = 0$, $k \neq k'$, which gives

$$\sigma^2 = \sum_k (A_k^h)^2 \langle (I_k^z)^2 \rangle. \quad (\text{D2})$$

Using $\langle (I_k^z)^2 \rangle = I^k(I^k + 1)/3$ for an infinite-temperature state, $A_k^h = A_{\text{lr}}^k v_0 |\phi(\mathbf{R}_k)|^2$, and assuming that the nuclear isotopic species with abundances v_j are distributed uniformly throughout the dot gives

$$\sigma^2 = \frac{1}{3} I_0 \sum_j v_j l^j (l^j + 1) (A_h^j)^2, \quad (\text{D3})$$

where

$$I_0 = v_0^2 \sum_k |\phi(\mathbf{R}_k)|^4. \quad (\text{D4})$$

Assuming that the envelope function $\phi(\mathbf{r})$ varies slowly on the scale of the lattice, we replace the sum in Eq. (D4) by an integral:

$$v_0 \sum_k |\phi(\mathbf{R}_k)|^4 \rightarrow \int d^3r |\phi(\mathbf{r})|^4. \quad (\text{D5})$$

Inserting the envelope functions (A2) and (A3) for a quantum dot with height a_z and radius l and evaluating the integral in Eq. (D5), we find

$$I_0 = \frac{3}{4} \frac{1}{N}. \quad (\text{D6})$$

Here, N is the number of nuclear spins within the quantum dot, given explicitly by

$$N = \frac{\pi l^2 a_z}{v_0}. \quad (\text{D7})$$

Inserting Eq. (D6) into Eq. (D3) directly gives Eq. (9).

-
- ¹D. Loss and D. P. DiVincenzo, *Phys. Rev. A* **57**, 120 (1998).
²V. Cerletti, W. A. Coish, O. Gywat, and D. Loss, *Nanotechnology* **16**, R27 (2005).
³G. Burkard, D. Loss, and D. P. DiVincenzo, *Phys. Rev. B* **59**, 2070 (1999).
⁴I. A. Merkulov, A. L. Efros, and M. Rosen, *Phys. Rev. B* **65**, 205309 (2002).
⁵A. V. Khaetskii, D. Loss, and L. Glazman, *Phys. Rev. Lett.* **88**, 186802 (2002).
⁶W. A. Coish and D. Loss, *Phys. Rev. B* **70**, 195340 (2004).
⁷J. R. Petta, A. C. Johnson, J. M. Taylor, E. A. Laird, A. Yacoby, M. D. Lukin, C. M. Marcus, M. P. Hanson, and A. C. Gossard, *Science* **309**, 2180 (2005).
⁸D. Heiss, S. Schaeck, H. Huebl, M. Bichler, G. Abstreiter, J. J. Finley, D. V. Bulaev, and D. Loss, *Phys. Rev. B* **76**, 241306(R) (2007).
⁹B. D. Gerardot, D. Brunner, P. A. Dalgarno, P. Öhberg, S. Seidl, M. Kroner, K. Karrai, N. G. Stoltz, P. M. Petroff, and R. J. Warburton, *Nature (London)* **451**, 441 (2008).
¹⁰A. J. Ramsay, S. J. Boyle, R. S. Kolodka, J. B. B. Oliveira, J. Skiba-Szymanska, H. Y. Liu, M. Hopkinson, A. M. Fox, and M. S. Skolnick, *Phys. Rev. Lett.* **100**, 197401 (2008).
¹¹B. Eble, C. Testelin, P. Desfonds, F. Bernardot, A. Balocchi, T. Amand, A. Miard, A. Lemaitre, X. Marie, and M. Chamorro, arXiv:0807.0968 (unpublished).
¹²Y. Komijani, M. Csontos, T. Ihn, K. Ensslin, D. Reuter, and A. Wieck, arXiv:0809.1362 (unpublished).
¹³M. Syperek, D. R. Yakovlev, A. Greilich, J. Misiewicz, M. Bayer, D. Reuter, and A. D. Wieck, *Phys. Rev. Lett.* **99**, 187401 (2007).
¹⁴T. Flissikowski, I. A. Akimov, A. Hundt, and F. Henneberger, *Phys. Rev. B* **68**, 161309(R) (2003).
¹⁵A. Shabaev, A. L. Efros, D. Gammon, and I. A. Merkulov, *Phys. Rev. B* **68**, 201305(R) (2003).
¹⁶L. M. Woods, T. L. Reinecke, and R. Kotlyar, *Phys. Rev. B* **69**, 125330 (2004).
¹⁷D. V. Bulaev and D. Loss, *Phys. Rev. Lett.* **95**, 076805 (2005).
¹⁸S. Laurent, B. Eble, O. Krebs, A. Lemaitre, B. Urbaszek, X. Marie, T. Amand, and P. Voisin, *Phys. Rev. Lett.* **94**, 147401 (2005).
¹⁹D. V. Bulaev and D. Loss, *Phys. Rev. Lett.* **98**, 097202 (2007).
²⁰Y. A. Serebrennikov, *Phys. Lett. A* **372**, 3307 (2008).
²¹G. Burkard, *Nature Mater.* **7**, 100 (2008).
²²D. Klauser, W. A. Coish, and D. Loss, *Phys. Rev. B* **73**, 205302 (2006).
²³A. Greilich, D. R. Yakovlev, A. Shabaev, Al. L. Efros, I. A. Yugova, R. Oulton, V. Stavarache, D. Reuter, A. Wieck, and M. Bayer, *Science* **313**, 341 (2006).
²⁴D. Stepanenko, G. Burkard, G. Giedke, and A. Imamoglu, *Phys. Rev. Lett.* **96**, 136401 (2006).
²⁵G. Giedke, J. M. Taylor, D. D'Alessandro, M. D. Lukin, and A. Imamoglu, *Phys. Rev. A* **74**, 032316 (2006).
²⁶A. Greilich, A. Shabaev, D. R. Yakovlev, Al. L. Efros, I. A. Yugova, D. Reuter, A. D. Wieck, and M. Bayer, *Science* **317**, 1896 (2007).
²⁷D. J. Reilly, J. M. Taylor, J. R. Petta, C. M. Marcus, M. P. Hanson, and A. C. Gossard, *Science* **321**, 817 (2008).
²⁸A. M. Stoneham, *Theory of Defects in Solids* (Oxford University Press, New York, 1972), Chap. 13.
²⁹R. Winkler, *Spin-Orbit Coupling Effects in Two-Dimensional Electron and Hole Systems*, Springer Tracts in Modern Physics Vol. 191 (Springer-Verlag, Berlin, 2003), Chap. 3.
³⁰P. Y. Yu and M. Cardona, *Fundamentals of Semiconductors* (Springer-Verlag, Berlin, 2005), Sec. 2.6.
³¹E. Clementi and D. L. Raimondi, *J. Chem. Phys.* **38**, 2686 (1963).
³²A. Abragam, *The Principles of Nuclear Magnetism* (Oxford University Press, New York, 1961), Sec. VI.II.
³³X. Marie, T. Amand, P. Le Jeune, M. Paillard, P. Renucci, L. E. Golub, V. D. Dymnikov, and E. L. Ivchenko, *Phys. Rev. B* **60**, 5811 (1999).
³⁴F. H. L. Koppens, D. Klauser, W. A. Coish, K. C. Nowack, L. P. Kouwenhoven, D. Loss, and L. M. K. Vandersypen, *Phys. Rev. Lett.* **99**, 106803 (2007); see especially the associated auxiliary material, EPAPS Document No. E-PRLTAO-99-027736 for the derivation of the decay of driven Rabi oscillations. For more information on EPAPS, see <http://www.aip.org/pubservs/epaps.html>.
³⁵D. Paget, G. Lampel, B. Sapoval, and V. I. Safarov, *Phys. Rev. B* **15**, 5780 (1977).
³⁶M. Gueron, *Phys. Rev.* **135**, A200 (1964).
³⁷R. Winkler, *Spin-Orbit Coupling Effects in Two-Dimensional*

Electron and Hole Systems, Springer Tracts in Modern Physics Vol. 191 (Springer-Verlag, Berlin, 2003), Appendix B–D.

³⁸I. Vurgaftman, J. R. Meyer, and L. R. Ram-Mohan, *J. Appl. Phys.* **89**, 5815 (2001).

³⁹Y. Yafet, *J. Phys. Chem. Solids* **21**, 99 (1961).

⁴⁰In Winkler's notation (Ref. [37](#)) these are the terms proportional

to C , B_{7v} , and B_{8v}^{\pm} . These terms will not lead to considerable corrections for our purposes. However, the terms Ck_{\pm} could become relevant when considering higher-order effects in the spin-orbit interaction, such as the cubic Dresselhaus terms which were derived in Ref. [17](#).